ACS OMEGA

http://pubs.acs.org/journal/acsodf

Article

Reduced Defects and Enhanced Performance of $(FAPbI_3)_{0.97}(MAPbBr_3)_{0.03}$-Based Perovskite Solar Cells by Trimesic Acid Additives

Hoang V. Quy, Dang H. Truyen, Sangmo Kim, and Chung W. Bark*

Cite This: *ACS Omega* 2021, 6, 16151−16158

Read Online

ACCESS | Metrics & More | Article Recommendations

ABSTRACT: A high-quality organolead trihalide perovskite film with large-sized crystalline grains and smooth surfaces is required to obtain efficient perovskite solar cells (PSCs). Herein, high-quality $(FAPbI_3)_{0.97}(MAPbBr_3)_{0.03}$ perovskite films were fabricated using trimesic acid (TMA) additives in a halide perovskite precursor solution to obtain efficient PSCs. The X-ray diffraction analysis and scanning electron microscopy of the films revealed that the TMA had a significant effect on the roughness of the films by acting as a surface link, thus reducing the surface defects and recombination at the grain boundaries. In addition, with the addition of the TMA additive, a smooth perovskite film with a flat surface and no pinholes was obtained. The perovskite film was used to fabricate a PSC device, and the device exhibited a high power conversion efficiency of 17.26%, which was higher than that of the control device (15.15%) under the same conditions. This study demonstrates a facile method to passivate defects on the perovskite layer via surface modification.

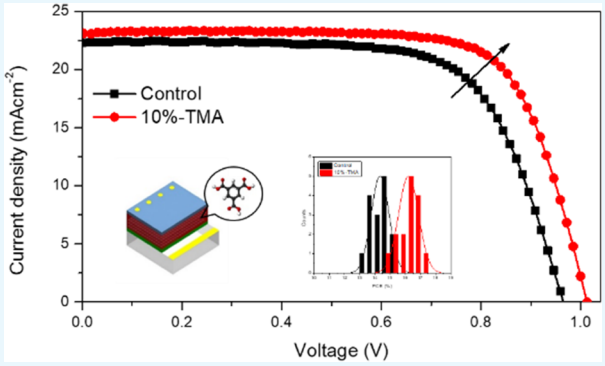

1. INTRODUCTION

Recently, organic−inorganic hybrid lead perovskite solar cells (PSCs) have attracted tremendous attention due to their splendid optoelectronic properties and their facile and cheap fabrication process.[1−5] $FAPbI_3$ perovskite is considered an ideal candidate for the fabrication of efficient and stable PSCs owing to its thermal stability and a low band gap (1.45 eV), which enables the broader absorption of ions of the solar spectrum.[6−8] $FAPbI_3$ consists of two phases: pure-phase black α-$FAPbI_3$ and photoinactive yellow δ-$FAPbI_3$, which is stable at room temperature. The yellow δ-$FAPbI_3$ reduces the crystallinity of $FAPbI_3$ films, thus hindering electron transport and reducing the efficiency of PSCs. The quality of perovskite films, which can be influenced by the preparation method, makes a significant contribution to the device capacity of PSCs.[9−11] However, owing to the difficulties in controlling these perovskite films including their organic components, rough and inhomogeneous films, which are sensitive to air, are formed.[12−14] The modification of the perovskite surface by enhancing the crystallinity, suppressing the surface defects, and reducing the number of pinholes has emerged as a powerful method to improve the film quality of perovskites. In the previous research, our group modified the perovskite surface by inserting an ultrathin NiO@C interfacial layer on the top of the perovskite layer, achieving a high efficiency of 15.78% in the planar n−i−p structure.[15,16]

Tremendous attempts have been devoted to modifying the specific characteristics of perovskite films by developing new preparation processes, such as one- or two-step solution methods, additive engineering, and antisolvent treatment, to obtain efficient and stable PSCs.[1,17−20] For example, halide perovskite films have been widely synthesized by solution-based bottom-up methods for precisely controlling the morphology of the films with large surface areas and high crystalline grain boundaries.[12,21−23] However, these unstable large-sized grain perovskite cuboids are highly sensitive to moisture, thus resulting in the quick degradation of the performance of PSCs. To overcome this disadvantage, the additive-based approach has emerged as an effective strategy to passivate surface defects. This approach improves the efficiency and stability of PSCs by improving the morphology and optoelectronic properties of mixed-perovskite devices. Recently, trimesic acid (TMA) has been used in a PbI_2 solution to improve the thermal stability and air stability of bulk $MAPbI_3$ perovskite films.[24] Trap-state passivation by non-

Received: April 16, 2021
Accepted: May 27, 2021
Published: June 10, 2021

https://doi.org/10.1021/acsomega.1c01909
ACS Omega 2021, 6, 16151−16158

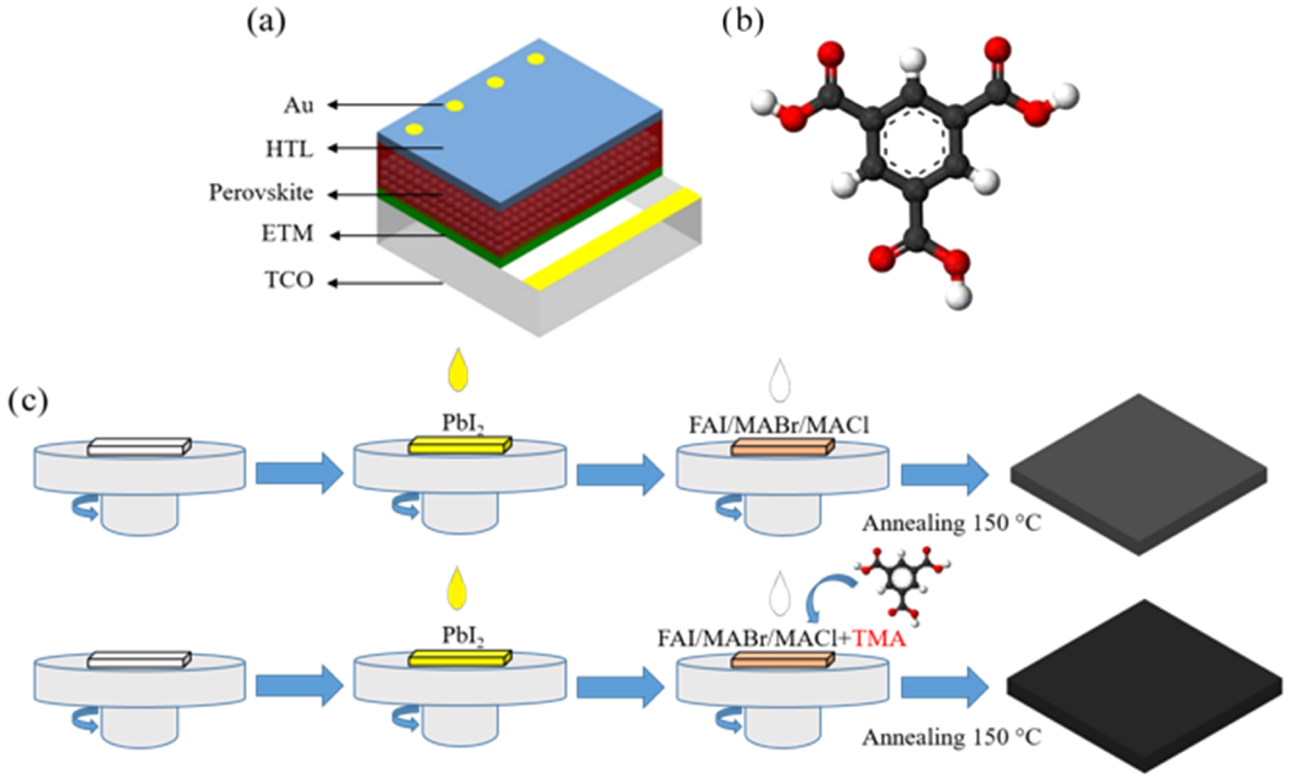

Figure 1. (a) Architecture of the mesoporous PSCs. (b) 3D chemical structure of the TMA additive. (c) Schematic illustration of the experimental process for the fabrication of the absorber layer using a two-step deposition process.

volatile small molecules was investigated with carboxylic acid groups by benzoic acid, p-phthalic acid, and trimesic acid to improve the performance of perovskite solar cells to 15.81%.[25] To our knowledge, there were no reports investigating the TMA additive directly in the hygroscopic organic such as methylammonium (MA+) and formanidium (FA+), which could affect the surface of the perovskite layer.

Herein, we employed an optimal amount of TMA to investigate the functions of additives on the surface of perovskite films. We found that the presence of a TMA additive played an important role in controlling the grain size and quality of the perovskite films.[18,26,27] In addition, the TMA additive induced the growth of a uniform perovskite on the perovskite film, thus suppressing surface defects and reducing carrier recombination at the grain boundaries. Furthermore, the optimal TMA concentration for obtaining a high-quality perovskite film was 10 wt %. The high-quality perovskite film was used to fabricate a PSC, and the device achieved a maximum power conversion efficiency (PCE) of 17.26%, which is higher than that of the control PSC 15.15%.

2. RESULTS AND DISCUSSION

To accurately investigate the effect of the TMA additive on the PSCs, a batch of 15 devices was fabricated under various TMA conditions. Herein, mesoscopic PSCs with a structure of fluorine-doped tin oxide (FTO)/cp-TiO_2/mp-TiO_2/(FAPbI$_3$)$_{0.97}$(MAPbBr$_3$)$_{0.03}$/spiro-OMeTAD/Au were designed. The schematic illustration of the architecture of the mesoscopic PSCs is shown in Figure 1a. The thickness of the absorber thin film was approximately 350 nm. A low band gap $FAPbI_3$ was selected to fabricate the PSCs to increase the light-harvesting potential of the device. The three-dimensional (3D) molecular structure of TMA including the benzene ring and three carboxyl groups is shown in Figure 1b. TMA was added as an additive to the perovskite layer to investigate its effects on the optical and performance properties of PSCs. Figure 1c shows the schematic illustration of the addition of TMA during the fabrication of the (FAPbI$_3$)$_{0.97}$(MAPbBr$_3$)$_{0.03}$-based PSCs by a two-step deposition method.

To understand the interaction between TMA and the perovskite, Fourier transform infrared spectroscopy (FTIR) was carried out to verify the presence of TMA in the control perovskite film and the 10%-TMA additive perovskite film as a representative sample. As shown in Figure 2, a strong peak can be observed at 1714 cm^{-1} in the control and modified

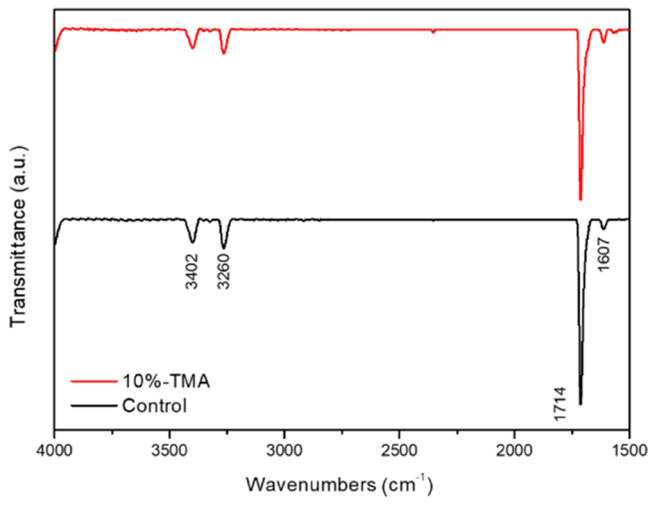

Figure 2. FTIR spectra of the pure TMA and TMA-additive perovskite films.

https://doi.org/10.1021/acsomega.1c01909
ACS Omega 2021, 6, 16151−16158

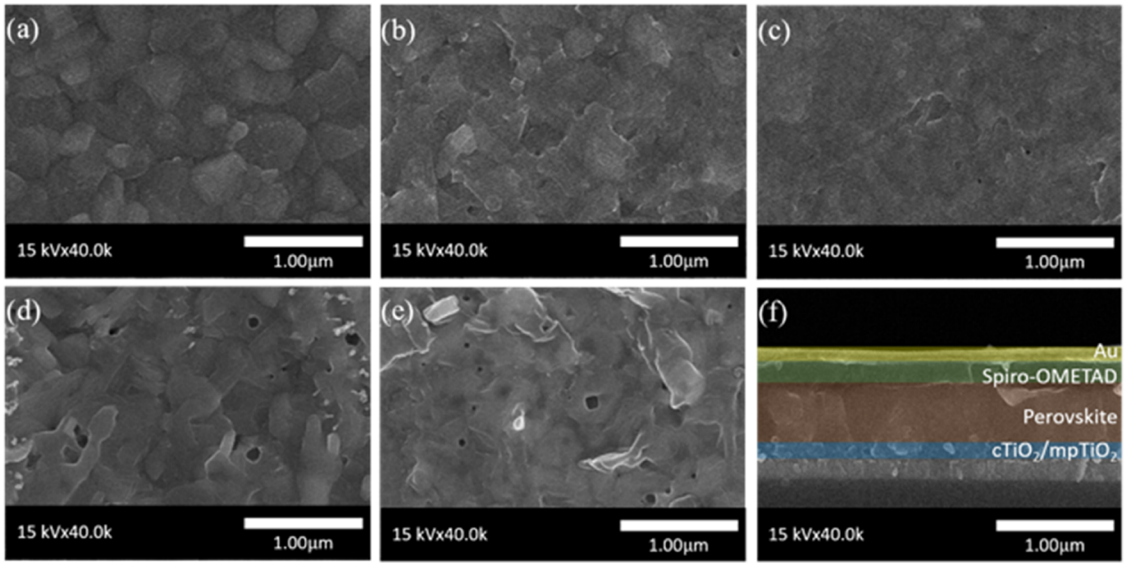

Figure 3. (a–e) Top-view field emission scanning electron microscopy (FE-SEM) images of the perovskite films modified with different concentrations of TMA: 0%, 5%, 10%, 15%, and 20%. (f) Cross-sectional SEM image of the PSC device.

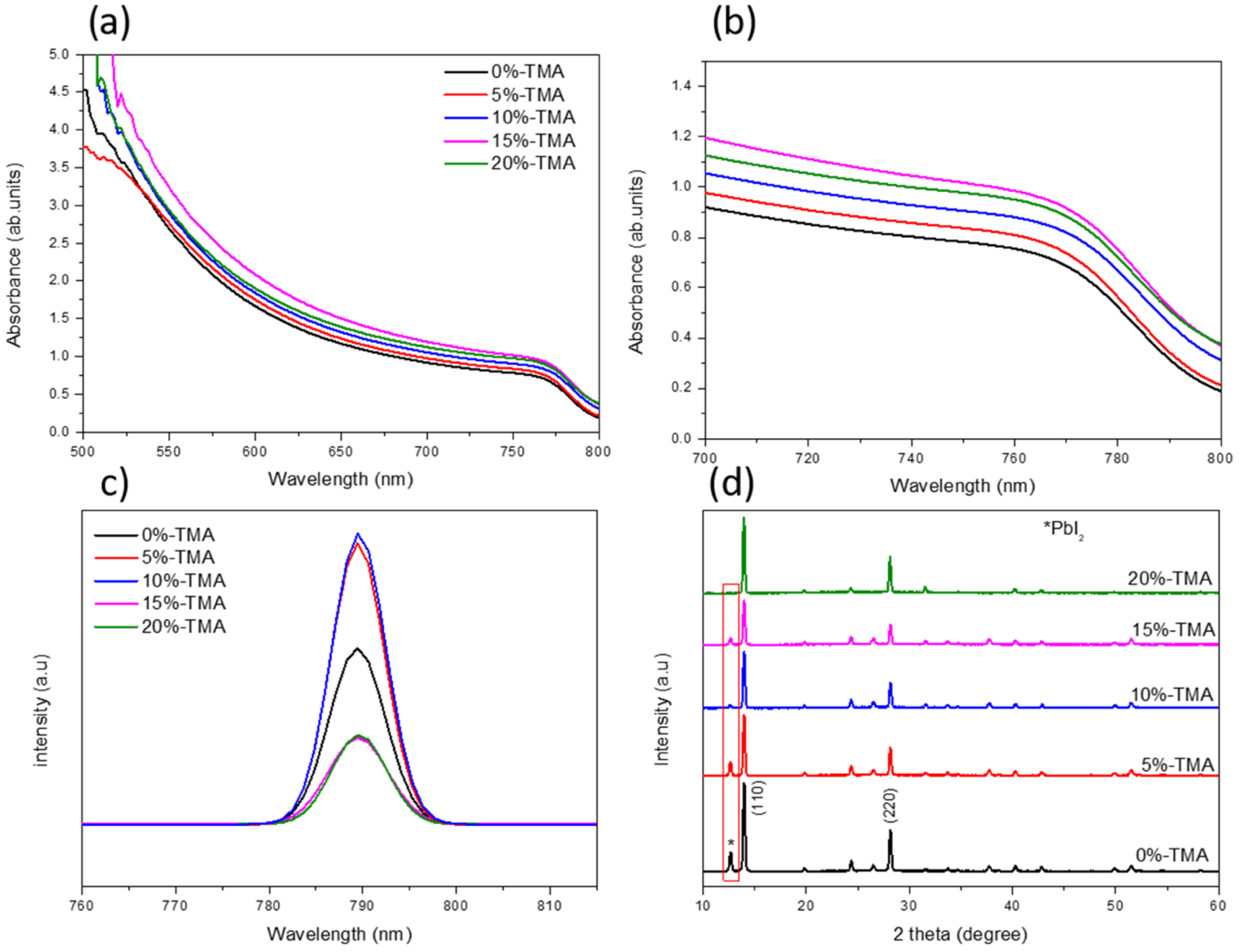

Figure 4. (a) UV–vis absorption spectra of the control FAPbI3 film and the TMA-modified perovskite film; (b) zoom-in view near the absorbance edge; (c) PL spectrum of the perovskite deposited on glass; and (d) XRD patterns of the perovskite film and perovskite films modified with 5%-, 10%-, 15%-, and 20%-TMA additives.

https://doi.org/10.1021/acsomega.1c01909
ACS Omega 2021, 6, 16151–16158

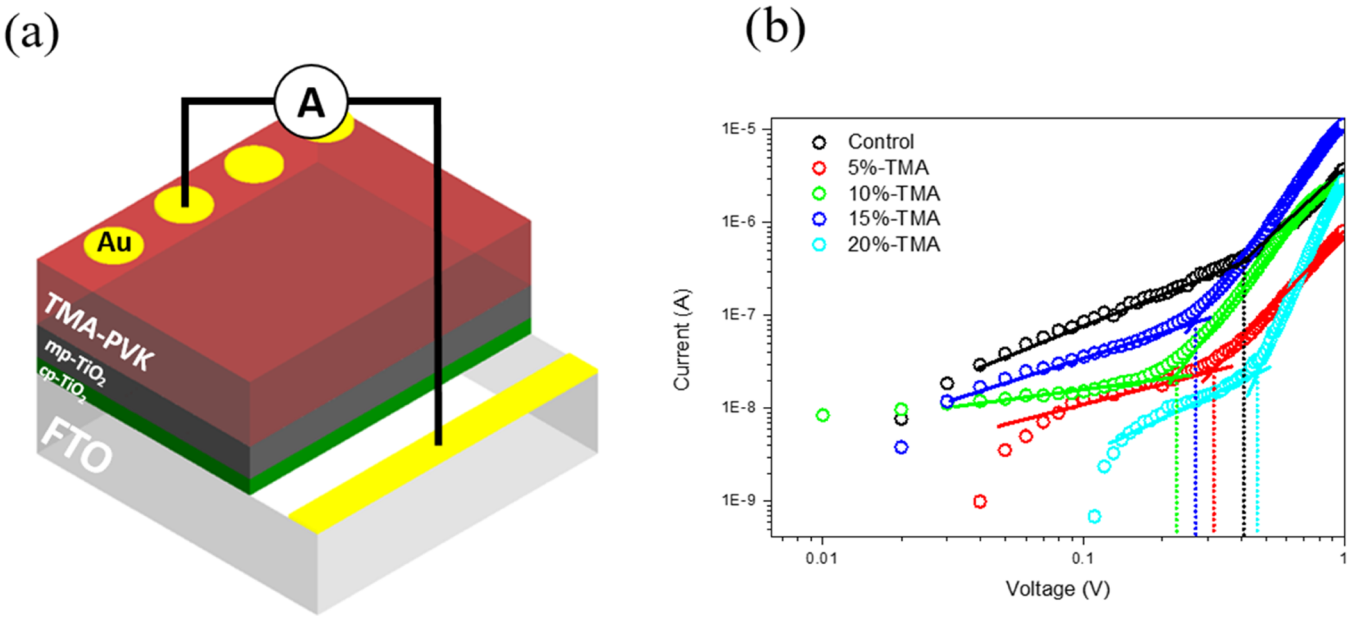

Figure 5. (a) Sample structure for trap density measurement. (b) Dark $I-V$ curves of the electron-only devices and fabricated using perovskite films modified with different concentrations of TMA: 0%, 5%, 10%, 15%, and 20%.

perovskite films, which corresponded to the strong stretching vibration of C═N from FA^+. In addition, two additional peaks were observed at 3402 and 3260 cm^{-1}, which could be attributed to the stretching vibration of N−H.[28] The FTIR spectrum of the TMA perovskite film is similar to that of the $(FAPbI_3)_{0.97}(MAPbBr_3)_{0.03}$ film. No new stretching vibration peak was observed during the reaction, indicating that the carboxylic acid group of the TMA was not inserted into the film but affected the perovskite surface.[29]

The $(FAPbI_3)_{0.97}(MAPbBr_3)_{0.03}$ perovskite thin films were fabricated by a two-step spin-coating process, and the size and shape of the crystal grains were significantly influenced by the TMA concentration. Figure 3a−f shows scanning electron microscopy (SEM) images of the original perovskite film (as control) and the perovskite films with 5%-, 10%-, 15%-, and 20%-TMA additives. As shown in the SEM image, the crystal grains of the pristine $(FAPbI_3)_{0.97}(MAPbBr_3)_{0.03}$ films exhibited clear boundaries with an average grain size of approximately 300 nm. After the addition of 5%- and 10%-TMA additives, the perovskite layer exhibited a uniform and smooth surface with a lower surface roughness, which reduced the recombination sites and improved the charge carrier mobility. However, with a further increase in the TMA concentration to 15% and 20%, a poor-quality perovskite surface with pinholes and large cuboids was observed, suggesting that this TMA additive is ineffective for improving the morphology of the perovskite film.

The UV−visible (UV−vis) absorption spectra of the perovskite films are shown in Figure 4a,b. As shown in the image, the light absorption intensity of the perovskite films increases slightly with increasing TMA concentration owing to the increase in the size of the perovskite grain. The absorption edge of the perovskite films is almost unchanged with the presence of the TMA additive. The absorption of the modified perovskite films is stronger than the absorption of the pristine perovskite film. However, the absorption of the 20%-TMA perovskite film is lower than that of the 15%-TMA perovskite film, which is likely attributed to the defects in the surface of the film. As shown in Figure 4c, the steady-state photoluminescence (PL) spectra of the perovskite films with the maximum emission peak of the film at 790 nm were observed at an excitation of 530 nm, which is consistent with the reports of a previous study.[30] The luminescence emission peak depicts radiative recombination and nonradiative decay.[31] A further increase in the peak intensity indicates the reduction of surface defects, which could suppress the recombination at the perovskite/HTL interface.[32−36] This is consistent with the SEM images and UV−vis absorption spectra. However, the perovskite films with 15- and 20%-TMA additives exhibited weak-intensity PL peaks, indicating the poor morphology of the films with several pinholes and smaller perovskite grains, which resulted in the reduction of the PCEs. Figure 4d shows the X-ray diffraction (XRD) patterns of the films with various TMA contents recorded from 10 to 60°. The 2θ peaks at 13.95, 19.83, 24.45, 28.12, 33.84, 34.81, 40.27, and 42.85° in the XRD patterns of the $(FAPbI_3)_{0.97}(MAPbBr_3)_{0.03}$ films confirmed the existence of the $FAPbI_3$ perovskite phase in the fabricated films. However, in the perovskite films with 15%- and 20%-TMA additives, the weak-intensity PL peaks explain the poor morphology with more pinholes and smaller perovskite grains, which results in the reduction in PCEs.[37,38] In addition, the peak observed at 12.63° in the XRD pattern of the pristine $FAPbI_3$ perovskite film without the TMA additive corresponded to the incomplete reaction between PbI_2 and formamidinium iodide (FAI) prepared using a stoichiometric precursor. With the addition of 10%-TMA, the peak at approximately 12.63° decreased; however, with an increase in the TMA content to 15%, the peak intensity increased. In contrast, the peak intensity at approximately 12.63° decreased with a further increase in the TMA content beyond 20%. These changes in the XRD results confirmed that the PbI_2 phase was strongly influenced by the concentration of the TMA additive. Therefore, the performance enhancement by the TMA additive could be attributed to the suppression of the surface defects.[24]

https://doi.org/10.1021/acsomega.1c01909
ACS Omega 2021, 6, 16151−16158

We investigate the control and modified electron-only device's electronic trap states using the space−charge−limited current (SCLC) technique. Figure 5a shows the sample structure for this measurement, while Figure 5b shows the dark current−voltage (I−V) analysis for control and modified perovskite devices. At the low voltage, an ohmic response of the electron-only devices was confirmed by the fit to $I = V$ (linear). At the high voltage, the current shows a significant increase for perovskite films modified with 0%-, 5%-, 10%-, 15%-, and 20%-TMA additives at V_{TFL} = 0.42, 0.32, 0.22, 0.27, and 0.47 V, respectively. The trap-state density is calculated using the following equation

$$V_{TFL} = \frac{en_{traps}L^2}{2\varepsilon\varepsilon_0} \quad (1)$$

where e is elementary of the electron, L is the thickness between the two metal contacts, ε is the relative dielectric constant of perovskite (26), ε_0 is the vacuum permittivity, and n_{traps} is the trap-state density. Correspondingly, we found that the control device has a trap density n_{traps} = 3.6 × 1015 cm^{-3}, while 10%-TMA perovskite film shows a low trap density n_{traps} = 1.88 × 1015 cm^{-3}.[20,39] Clearly, using a 10%-TMA additive effectively passivates electron traps, leading to the formation of a high-quality perovskite layer.

The effect of TMA on the photovoltaic properties of the PSCs is summarized in Table 1. Figure 6a−d shows the statistical distribution of the open-circuit voltage (V_{OC}), short-circuit current density (J_{SC}), fill factor (FF), and PCE of the control and TMA additive-perovskite-based devices. The control device without TMA exhibited a J_{SC} of 21.84 mA·cm^{-2}, a V_{OC} of 0.95 V, a FF of 0.73, and a PCE of 15.15%. The high efficiency of the TMA additive in the perovskite-based device could be related to the excellent quality of the absorber layer. Moreover, an additive of $MAPbBr_3$ was employed in the perovskite layer to enhance the stabilization of the α-$FAPbI_3$ phase. The addition of TMA to $(FAPbI_3)_{0.97}(MAPbBr_3)_{0.03}$ perovskite increased the overall efficiency of all of the PSC devices. The perovskite film with a 10%-TMA additive exhibited the champion PCE of 17.26% with a V_{OC} of 1.01 V, a J_{SC} of 23.11 mA·cm^{-2}, and a FF of 0.74, indicating that the optimum TMA content was 10% (Table 1, Figure 6e). The enhanced efficiency of the PSC owing to the increased values of V_{OC} and FF could be attributed to the improved optical properties, good quality of the perovskite film, and lower series resistance (Table 1). The enhanced FF of the modified perovskite films could be assigned to the surface flatness of the perovskite films, which improved the charge-transfer property.[40] However, with an increase in the TMA concentration to 20%, the PCE values decreased to 15.28%, which could be attributed to the formation of a coarse perovskite film with several pinholes. Figure 6f shows the current density−voltage (J−V) curves of the optimum PSC device (10%-TMA), which are consistent with those of the discussed results.

Table 1. Photovoltaic Performance of PSCs with Various Amounts of TMA Based on 75 Cells

PSCs	J_{SC} (mA·cm^{-2})	V_{OC} (V)	FF	PCE (%)	Rs
control	21.84	0.95	0.73	15.15	148
5%-TMA	23.94	0.99	0.69	16.46	142
10%-TMA	23.11	1.01	0.74	17.26	120
15%-TMA	22.49	0.99	0.71	15.91	127
20%-TMA	20.96	1.00	0.72	15.28	139

Figure 7a exhibits the external quantum efficiency (EQE) spectra of the control and 10%-TMA-based PSCs. The light response from the EQE spectra of the modified devices was approximately 90%, higher than those of the control samples. This could be assigned to the improved optical properties and reduced charge recombination at the hole transport layer/perovskite interface owing to the flat surface of the perovskite layer. The integrated J_{SC} values of the control and 10%-TMA-based PSCs from the EQE spectra were 23.5 and 22.5 mA·cm^{-2}, respectively, which are highly consistent with the measured J_{SC}. The histogram of each device was fitted with a normal distribution model, as shown in Figure 7b. Both histograms illustrate that the 10%-TMA additive in perovskite-based devices exhibited enhanced solar cell performance.

3. CONCLUSIONS

In conclusion, a modified procedure for absorber layers with a TMA additive at different concentrations was developed to fabricate high-quality perovskite films using a two-step deposition method. By varying the amount of TMA in the perovskite precursor solutions, a significant enhancement of the PCE from 15.15 to 17.26% was obtained at a TMA concentration of 10 wt%. This improvement was based on the improved quality of the perovskite film owing to the flat surface, lack of pinholes, and low series resistance, which enhanced the J_{SC} and V_{OC}. Furthermore, the 10 wt %-TMA additive-based devices exhibited a suppressed hysteresis effect compared to the control device. The improved performance could be attributed to the presence of the TMA additive in the perovskite precursor solution during the perovskite formation process. The findings of this study indicate that the efficiency of mesoscopic PSCs can be further improved by modifying the absorber film via the addition of additives.

4. EXPERIMENTAL SECTION

4.1. Reagents and Materials. Titanium diisopropoxide bis(acetylacetone) (75 wt % in isopropanol, Sigma-Aldrich), butyl alcohol (99%, Sigma-Aldrich), TiO_2 (Dyesol NT-18, Dyesol, Australia), absolute alcohol (≥99.5%, Sigma-Aldrich), lead(II) iodide (99.999% trace metals basic, Sigma-Aldrich), *N*,*N*-dimethylformamide (DMF, 99.8%, Sigma-Aldrich), dimethyl sulfoxide (DMSO, ≥99.9%, Sigma-Aldrich), trimesic acid (TMA; benzene-1,3,5-tricarboxylic acid, 95%, Sigma-Aldrich), formamidinium iodide (FAI, greatcellsolar, Australia), methylammonium bromide (MABr, Sigma-Aldrich), methylammonium hydrochloride (MACl, Sigma-Aldrich), 2-propanol (anhydrous, 99.5%, Sigma-Aldrich), chlorobenzene (99.8%, Sigma-Aldrich), acetonitrile (99.93%, Sigma-Aldrich), and 2,2′,7,7′-tetrakis[*N*,*N*-di(4-methoxyphenyl)amino]-9,9′-spirobifluorene (spiro-OMeTAD, 99%, Sigma-Aldrich), 4-*tert*-butylpyridine (98%, Sigma-Aldrich), bis(trifluoromethane)-sulfonimide lithium salt (Li-TSFI; ≥99.0%, Sigma-Aldrich) were used. All reagents were used as received without any further purification.

4.2. Device Preparation. Briefly, a glass/FTO substrate (7 Ω sq^{-1}) was cleaned consecutively with isopropanol, acetone, distilled water, and ethanol, then dried under a N_2 flow, and finally treated with UV ozone for 15 min. Subsequently, a TiO_2 blocking layer was spin-coated on the washed FTO substrate at 2000 rpm for 20 s using 0.15 M titanium diisopropoxide

https://doi.org/10.1021/acsomega.1c01909
ACS Omega 2021, 6, 16151−16158

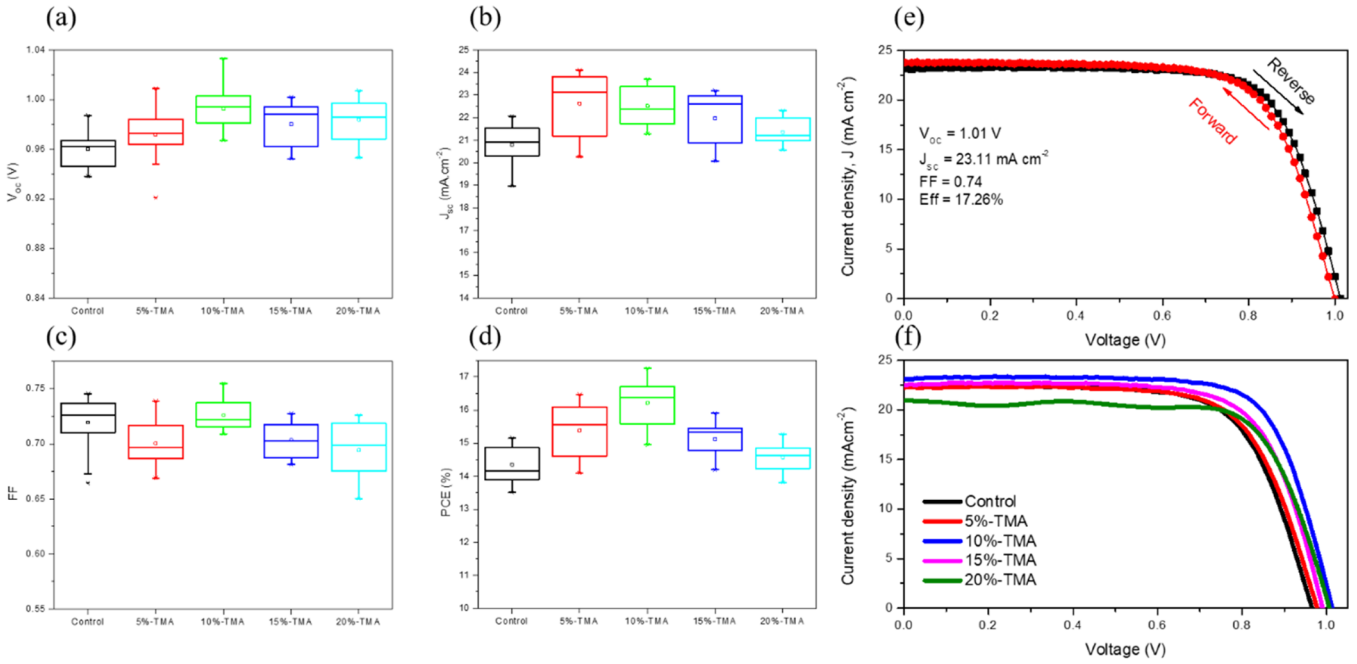

Figure 6. (a–d) Statistical distribution of the PCE, J_{SC}, V_{OC}, and FF of the control PSC and the TMA-modified perovskite-based PSCs. Data were collected from 75 cells. (e) Current density–voltage curve of the best cell obtained using 10% TMA. (f) Photocurrent density–voltage curve of the TMA-modified $FAPbI_3$-based PSCs at different TMA concentrations.

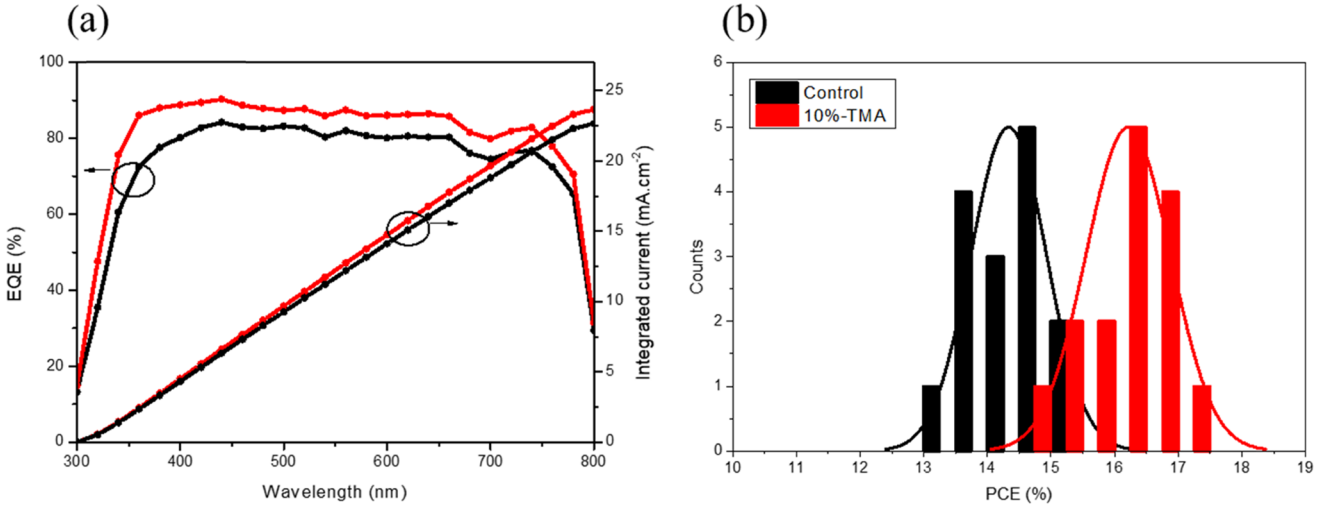

Figure 7. (a) EQE spectra of the control and 10%-TMA-based PSCs. (b) PCE distribution of the 30 PSC devices.

bis(acetylacetone) (75% in 1-butanol) in 1-butanol solution, which was heated at 125 °C for 15 min. After cooling to room temperature, the porous layer with a TiO_2 paste was diluted in ethanol (1:6, wt/wt), after which the paste was spin-coated on the TiO_2 compact layer at 4000 rpm for 20 s, followed by annealing at 480 °C for 30 min. The perovskite layer was deposited by performing a two-step spin-coating deposition method under a N_2 atmosphere in a glovebox. First, a PbI_2 solution (1.3 M) was prepared by dissolving 600 mg of PbI_2 in 900 μL of DMF and 100 μL of DMSO, after which the mixture was stirred at room temperature for 1 day. Subsequently, 50 μL of PbI_2 was spin-coated on the mesoporous TiO_2 film at 2000 rpm for 20 s (without loading time). The mixture solution of FAI/MABr/MACl (60:6:6, mg) without and with a certain amount of TMA (mass ratio of TMA vs FAI) in 2-propanol was spin-coated onto the PbI_2-coated substrate for 20 s (loading time) at 4000 rpm for 20 s and dried at 150 °C for 15 min. Subsequently, 50 μL of the spiro-OMeTAD solution was dropped on the absorber layer at 3000 rpm for 30 s, where 72.3 mg of spiro-MeOTAD was dissolved in 1 mL of chlorobenzene with the addition of 28.8 μL of 4-*tert*-butylpyridine and 17.5 μL of Li-TFSI solution (52 mg of Li-TSFI in 100 μL of acetonitrile). Finally, 80 nm of gold was evaporated on the spiro-OMeTAD film.

4.3. Device Characterization. The UV–vis absorption spectra were measured using an Agilent 8453 UV–vis spectrophotometer (Agilent 8453, Agilent Technologies, Santa Clara, CA). The XRD patterns of the films were obtained using an XRD Rigaku DMAX 2200 system (Rigaku, Tokyo, Japan) with Cu Kα (λ = 0.15406 nm) as the X-ray source. An infrared spectrometric analyzer (Vertex 70, Bruker, Ettlingen, Germany) was used to record the FTIR spectra. The

https://doi.org/10.1021/acsomega.1c01909
ACS Omega 2021, 6, 16151–16158

cross-sectional morphology and the surface of the films were characterized using a field emission scanning electron microscope (Hitachi S-4700, Tokyo, Japan) operated at 10 kV. The steady-state PL spectra of the films were determined using a QuantaMaster TM 50 PTI (Birmingham, New Jersey). The J–V curves of PSCs were measured under 1 sun illumination (AM1.5G, 100 mW·cm^{-2}), using a solar simulator (Polaromix K201, Solar simulator LAB 50, McScience K3000, McScience, Gyeonggi-do, Korea). The size of PSCs was calculated with an area of 0.053 cm^2 using a metal mask. The EQE was measured on a computer test controlling system (McScience, Gyeonggi-do, Korea) containing a xenon lamp power source.

AUTHOR INFORMATION

Corresponding Author

Chung W. Bark − *Department of Electrical Engineering, Gachon University, 13120 Seongnam, Korea;* orcid.org/0000-0002-9394-4240; Phone: 82-31-750-5351; Email: bark@gachon.ac.kr

Authors

Hoang V. Quy − *Department of Electrical Engineering, Gachon University, 13120 Seongnam, Korea*

Dang H. Truyen − *Department of Electrical Engineering, Gachon University, 13120 Seongnam, Korea*

Sangmo Kim − *School of Intelligent Mechatronics Engineering, Sejong University, 05006 Seoul, Korea*

Complete contact information is available at: https://pubs.acs.org/10.1021/acsomega.1c01909

Notes

The authors declare no competing financial interest.

ACKNOWLEDGMENTS

This work was supported by grants from the National Research Foundation of Korea (NRF) funded by the Ministry of Science and ICT (NRF-2020R1F1A1076576), the Korea Institute of Energy Technology Evaluation and Planning (KETEP), the Ministry of Trade, Industry & Energy (MOTIE) of the Republic of Korea (No. 20194030202290), and the Gachon University research fund of 2019 (GCU-2019-0800). The authors would like to thank the Smart Materials Research Center for IoT supported by the NFEC at Gachon University for its support and assistance with the SEM.

REFERENCES

(1) Chen, H.; Ye, F.; Tang, W.; He, J.; Yin, M.; Wang, Y.; Xie, F.; Bi, E.; Yang, X.; Grätzel, M.; et al. A solvent-and vacuum-free route to large-area perovskite films for efficient solar modules. *Nature* **2017**, *550*, 92−95.

(2) Jung, E. H.; Jeon, N. J.; Park, E. Y.; Moon, C. S.; Shin, T. J.; Yang, T.-Y.; Noh, J. H.; Seo, J. Efficient, stable and scalable perovskite solar cells using poly (3-hexylthiophene). *Nature* **2019**, *567*, 511−515.

(3) Wang, P.; Zhang, X.; Zhou, Y.; Jiang, Q.; Ye, Q.; Chu, Z.; Li, X.; Yang, X.; Yin, Z.; You, J. Solvent-controlled growth of inorganic perovskite films in dry environment for efficient and stable solar cells. *Nat. Commun.* **2018**, *9*, No. 2225.

(4) Wang, M.; Zang, Z.; Yang, B.; Hu, X.; Sun, K.; Sun, L. Performance improvement of perovskite solar cells through enhanced hole extraction: the role of iodide concentration gradient. *Sol. Energy Mater. Sol. Cells* **2018**, *185*, 117−123.

(5) NREL. Best Research-Cell Efficiences charthttps://www.nrel.gov/pv/assets/pdfs/best-research-cell-efficiencies.20200104.pdf.

(6) Aharon, S.; Dymshits, A.; Rotem, A.; Etgar, L. Temperature dependence of hole conductor free formamidinium lead iodide perovskite based solar cells. *J. Mater. Chem. A* **2015**, *3*, 9171−9178.

(7) Berhe, T. A.; Su, W.-N.; Chen, C.-H.; Pan, C.-J.; Cheng, J.-H.; Chen, H.-M.; Tsai, M.-C.; Chen, L.-Y.; Dubale, A. A.; Hwang, B.-J. Organometal halide perovskite solar cells: degradation and stability. *Energy Environ. Sci.* **2016**, *9*, 323−356.

(8) Fu, Y.; Wu, T.; Wang, J.; Zhai, J.; Shearer, M. J.; Zhao, Y.; Hamers, R. J.; Kan, E.; Deng, K.; Zhu, X.-Y.; et al. Stabilization of the metastable lead iodide perovskite phase via surface functionalization. *Nano Lett.* **2017**, *17*, 4405−4414.

(9) Li, Y.; Ji, L.; Liu, R.; Zhang, C.; Mak, C. H.; Zou, X.; Shen, H.-H.; Leu, S.-Y.; Hsu, H.-Y. A review on morphology engineering for highly efficient and stable hybrid perovskite solar cells. *J. Mater. Chem. A* **2018**, *6*, 12842−12875.

(10) Zhang, H.; Shi, J.; Zhu, L.; Luo, Y.; Li, D.; Wu, H.; Meng, Q. Polystyrene stabilized perovskite component, grain and microstructure for improved efficiency and stability of planar solar cells. *Nano Energy* **2018**, *43*, 383−392.

(11) Xiao, Y.; Han, G.; Wu, J.; Lin, J.-Y. Efficient bifacial perovskite solar cell based on a highly transparent poly (3, 4-ethylenedioxythiophene) as the p-type hole-transporting material. *J. Power Sources* **2016**, *306*, 171−177.

(12) Tan, H.; Jain, A.; Voznyy, O.; Lan, X.; De Arquer, F. P. G.; Fan, J. Z.; Quintero-Bermudez, R.; Yuan, M.; Zhang, B.; Zhao, Y.; et al. Efficient and stable solution-processed planar perovskite solar cells via contact passivation. *Science* **2017**, *355*, 722−726.

(13) Jo, Y.; Oh, K. S.; Kim, M.; Kim, K. H.; Lee, H.; Lee, C. W.; Kim, D. S. High performance of planar perovskite solar cells produced from PbI2 (DMSO) and PbI2 (NMP) complexes by intramolecular exchange. *Adv. Mater. Interfaces* **2016**, *3*, No. 1500768.

(14) Bi, D.; Yi, C.; Luo, J.; Décoppet, J.-D.; Zhang, F.; Zakeeruddin, S. M.; Li, X.; Hagfeldt, A.; Grätzel, M. Polymer-templated nucleation and crystal growth of perovskite films for solar cells with efficiency greater than 21%. *Nat. Energy* **2016**, *1*, No. 16142.

(15) Nguyen, T. M. H.; Bark, C. W. Highly porous nanostructured NiO@ C as interface-effective layer in planar nip perovskite solar cells. *J. Alloys Compd.* **2020**, *841*, No. 155711.

(16) Quy, H. V.; Truyen, D. H.; Kim, S.; Bark, C. W. Facile Synthesis of Spherical TiO2 Hollow Nanospheres with a Diameter of 150 nm for High-Performance Mesoporous Perovskite Solar Cells. *Materials* **2021**, *14*, No. 629.

(17) Zhang, F.; Zhu, K. Additive engineering for efficient and stable perovskite solar cells. *Adv. Energy Mater.* **2020**, *10*, No. 1902579.

(18) Li, X.; Dar, M. I.; Yi, C.; Luo, J.; Tschumi, M.; Zakeeruddin, S. M.; Nazeeruddin, M. K.; Han, H.; Grätzel, M. Improved performance and stability of perovskite solar cells by crystal crosslinking with alkylphosphonic acid ω-ammonium chlorides. *Nat. Chem.* **2015**, *7*, 703−711.

(19) Saliba, M.; Matsui, T.; Domanski, K.; Seo, J.-Y.; Ummadisingu, A.; Zakeeruddin, S. M.; Correa-Baena, J.-P.; Tress, W. R.; Abate, A.; Hagfeldt, A.; et al. Incorporation of rubidium cations into perovskite solar cells improves photovoltaic performance. *Science* **2016**, *354*, 206−209.

(20) Nguyen, T. M. H.; Kim, S.; Bark, C. W. Solution-processed and self-powered photodetector in vertical architecture using mixed-halide perovskite for highly sensitive UVC detection. *J. Mater. Chem. A* **2021**, *9*, 1269−1276.

(21) Tsai, H.; Nie, W.; Blancon, J.-C.; Stoumpos, C. C.; Asadpour, R.; Harutyunyan, B.; Neukirch, A. J.; Verduzco, R.; Crochet, J. J.; Tretiak, S.; et al. High-efficiency two-dimensional Ruddlesden−Popper perovskite solar cells. *Nature* **2016**, *536*, 312−316.

(22) Jeon, N. J.; Na, H.; Jung, E. H.; Yang, T.-Y.; Lee, Y. G.; Kim, G.; Shin, H.-W.; Seok, S. I.; Lee, J.; Seo, J. A fluorene-terminated hole-transporting material for highly efficient and stable perovskite solar cells. *Nat. Energy* **2018**, *3*, 682−689.

(23) Grancini, G.; Roldán-Carmona, C.; Zimmermann, I.; Mosconi, E.; Lee, X.; Martineau, D.; Narbey, S.; Oswald, F.; De Angelis, F.;

Graetzel, M. One-Year stable perovskite solar cells by 2D/3D interface engineering. *Nat. Commun.* **2017**, *8*, No. 15684.
(24) Su, L.; Xiao, Y.; Han, G.; Lu, L.; Li, H.; Zhu, M. Performance enhancement of perovskite solar cells using trimesic acid additive in the two-step solution method. *J. Power Sources* **2019**, *426*, 11−15.
(25) Guan, L.; Jiao, N.; Guo, Y. Trap-state passivation by nonvolatile small molecules with carboxylic acid groups for efficient planar perovskite solar cells. *J. Phys. Chem. C* **2019**, *123*, 14223−14228.
(26) Qiu, L.; Xing, K.; Zhang, J.; Yang, Y.; Cao, W.; Zhou, X.; Zhu, K.; Xia, D.; Fan, R. Two-Dimensional Metal−Organic Frameworks-Based Grain Termination Strategy Enables High-Efficiency Perovskite Photovoltaics with Enhanced Moisture and Thermal Stability. *Adv. Funct. Mater.* **2021**, *31*, No. 2010368.
(27) Zhao, J.; Li, H.; Li, C.; Zhang, Q.; Sun, J.; Wang, X.; Guo, J.; Xie, L.; Xie, J.; He, B.; et al. MOF for template-directed growth of well-oriented nanowire hybrid arrays on carbon nanotube fibers for wearable electronics integrated with triboelectric nanogenerators. *Nano Energy* **2018**, *45*, 420−431.
(28) Zhou, Z.; Pang, S.; Ji, F.; Zhang, B.; Cui, G. The fabrication of formamidinium lead iodide perovskite thin films via organic cation exchange. *Chem. Commun.* **2016**, *52*, 3828−3831.
(29) Medina-Velazquez, D.; Alejandre-Zuniga, B.; Loera-Serna, S.; Ortiz, E.; Morales-Ramirez, A. dJ.; Garfias-Garcia, E.; Garcia-Murillo, A.; Falcony, C. An alkaline one-pot reaction to synthesize luminescent Eu-BTC MOF nanorods, highly pure and water-insoluble, under room conditions. *J. Nanopart. Res.* **2016**, *18*, No. 352.
(30) Jiang, Q.; Zhang, L.; Wang, H.; Yang, X.; Meng, J.; Liu, H.; Yin, Z.; Wu, J.; Zhang, X.; You, J. Enhanced electron extraction using SnO2 for high-efficiency planar-structure HC (NH2)2PbI3-based perovskite solar cells. *Nat. Energy* **2017**, *2*, No. 16177.
(31) Yuan, D.-X.; Gorka, A.; Xu, M.-F.; Wang, Z.-K.; Liao, L.-S. Inverted planar NH2CH [double bond, length as m-dash] NH2PbI3 perovskite solar cells with 13.56% efficiency via low temperature processing. *Phys. Chem. Chem. Phys.* **2015**, *17*, 19745−19750.
(32) Duan, J.; Zhao, Y.; Yang, X.; Wang, Y.; He, B.; Tang, Q. Lanthanide ions doped CsPbBr3 halides for htm-free 10.14%-efficiency inorganic perovskite solar cell with an ultrahigh open-circuit voltage of 1.594 V. *Adv. Energy Mater.* **2018**, *8*, No. 1802346.
(33) de Quilettes, D. W.; Vorpahl, S. M.; Stranks, S. D.; Nagaoka, H.; Eperon, G. E.; Ziffer, M. E.; Snaith, H. J.; Ginger, D. S. Impact of microstructure on local carrier lifetime in perovskite solar cells. *Science* **2015**, *348*, 683−686.
(34) Al Mamun, A.; Ava, T. T.; Jeong, H. J.; Jeong, M. S.; Namkoong, G. A deconvoluted PL approach to probe the charge carrier dynamics of the grain interior and grain boundary of a perovskite film for perovskite solar cell applications. *Phys. Chem. Chem. Phys.* **2017**, *19*, 9143−9148.
(35) Swarnkar, A.; Chulliyil, R.; Ravi, V. K.; Irfanullah, M.; Chowdhury, A.; Nag, A. Colloidal CsPbBr3 perovskite nanocrystals: luminescence beyond traditional quantum dots. *Angew. Chem.* **2015**, *127*, 15644−15648.
(36) Li, J.; Yuan, X.; Jing, P.; Li, J.; Wei, M.; Hua, J.; Zhao, J.; Tian, L. Temperature-dependent photoluminescence of inorganic perovskite nanocrystal films. *RSC Adv.* **2016**, *6*, 78311−78316.
(37) Reyna, Y.; Salado, M.; Kazim, S.; Pérez-Tomas, A.; Ahmad, S.; Lira-Cantu, M. Performance and stability of mixed FAPbI3(0.85)-MAPbBr3(0.15) halide perovskite solar cells under outdoor conditions and the effect of low light irradiation. *Nano Energy* **2016**, *30*, 570−579.
(38) Zhang, M.; Wu, F.; Chi, D.; Shi, K.; Huang, S. High-efficiency perovskite solar cells with poly (vinylpyrrolidone)-doped SnO2 as an electron transport layer. *Mater. Adv.* **2020**, *1*, 617−624.
(39) Pammi, S.; Maddaka, R.; Tran, V.-D.; Eom, J.-H.; Pecunia, V.; Majumder, S.; Kim, M.-D.; Yoon, S. G. CVD-deposited hybrid lead halide perovskite films for high-responsivity, self-powered photodetectors with enhanced photo stability under ambient conditions. *Nano Energy* **2020**, *74*, No. 104872.
(40) Mei, Y.; Liu, H.; Li, X.; Wang, S. Hollow TiO2 spheres as mesoporous layer for better efficiency and stability of perovskite solar cells. *J. Alloys Compd.* **2020**, *866*, No. 158079.

https://doi.org/10.1021/acsomega.1c01909
ACS Omega 2021, 6, 16151−16158